Appl Phys B (2010) 100: 627–635
DOI 10.1007/s00340-010-4072-0

Applied Physics B
Lasers and Optics

QEPAS spectrophones: design, optimization, and performance

L. Dong · A.A. Kosterev · D. Thomazy · F.K. Tittel

Received: 26 April 2010 / Published online: 21 May 2010

Abstract The impact of design parameters of a spectrophone for quartz-enhanced photoacoustic spectroscopy on its performance was investigated. The microresonator of spectrophone is optimized based on an experimental study. The results show that a 4.4 mm-long tube with 0.6 mm inner diameter yields the highest signal-to-noise ratio, which is ∼30 times higher than that of a bare QTF at gas pressures between 400 and 800 Torr. The optimized configuration demonstrates a normalized noise-equivalent absorption coefficient (1σ) of 3.3×10^{-9} $cm^{-1}W/Hz^{1/2}$ for C_2H_2 detection at atmospheric pressure. The effect of the changing carrier gas composition is studied. A side-by-side sensitivity comparison between QEPAS and conventional photoacoustic spectroscopy technique is reported.

1 Introduction

The development of gas detection techniques and the design of rugged and compact gas sensors for environmental monitoring, industrial process control applications and medical diagnostics are of considerable interest [1–7]. In this paper we report a detailed study to improve a gas detection technology called quartz-enhanced photoacoustic spectroscopy (QEPAS), which was developed by Kosterev et al. [8, 9]. QEPAS sensor technology is based on a novel approach to photoacoustic detection which employs a quartz tuning fork (QTF) [10] as a resonant acoustic transducer. A QEPAS sensor detects a weak acoustic wave that is generated when optical radiation interacts with a trace gas. The pressure wave excites a resonant vibration of the QTF which is then converted into an electric signal due to the piezoelectric effect. Subsequently, the electric signal, which is proportional to the concentration of the gas, is measured by a transimpedance amplifier. QEPAS sensors have been used with various laser sources including near-infrared (NIR) and mid-infrared (MIR) semiconductor lasers (both distributed feedback and external cavity), optical parametric oscillators (OPO), and fiber amplifiers, and was applied to the detection of different chemical species including molecules with unresolved vibrational absorption bands [11–22]. Merits of QEPAS compared to conventional photoacoustic spectroscopy (PAS) include better QEPAS sensor immunity to environmental acoustic noise, a simple spectrophone design, and its capability to analyze trace-gas samples of ∼1 mm^3 in volume. These advantages make the QEPAS technology competitive with and in many cases preferred to other trace-gas sensing methods.

A commonly used QEPAS-based spectrophone consists of a QTF and a so-called microresonator (mR). The mR is formed by one or two thin tubes, and a QTF is positioned between or beside the tube(s) to probe the acoustic vibration excited in the gas contained inside the tubes. It was observed in initial studies that the use of a mR increases the QEPAS sensitivity 10 times or more. Furthermore, the mR isolates the QTF from accidental acoustic resonances in the sensor enclosure, which can otherwise distort the QEPAS signal. The mR in certain conditions such as low gas pressure or non-matched length acts simply as a confinement to the sound wave and does not exhibit a pronounced resonant behavior. However, at the practically important conditions of atmospheric gas pressure and carefully chosen dimensions the acoustic resonance in the mR tubes can significantly improve the sensor performance. In this paper we present an experimental investigation of the QEPAS sensor

L. Dong (✉) · A.A. Kosterev · D. Thomazy · F.K. Tittel
Electrical and Computer Engineering Department,
Rice University, 6100 Main St., Houston, TX 77005, USA
e-mail: lei.dong@rice.edu

operation as a function of the geometrical mR parameters and derive conclusions regarding the optimum mR configuration depending on a specific application. We also performed a side-by-side comparison of QEPAS with a QTF only, QEPAS with an optimized mR, and conventional PAS using a state-of-the-art differential acoustic cell.

2 QEPAS spectrophones

In conventional PAS, the acoustic resonator plays an important role [23]. The absorbed laser energy is accumulated in the acoustic mode of the resonator. The amplitude of the acoustic wave is scaled by the quality factor Q that is equal to the ratio between the energy accumulated in the resonator and the energy loss per cycle [24]. Typically the Q-factor of an acoustic resonator is 20–200, thus providing an essential gain in sensitivity. The microphone is coupled to the resonator through a small hole in a sidewall of the acoustic resonator. It can be usually considered as a broadband acoustic detector not exhibiting pronounced frequency selectivity. Hence, the acoustic resonator is the only frequency-selective element in the sensor. Its resonance can be tuned to any desired frequency within the wide microphone band (often, 20–20 000 Hz). Unlike a microphone, the QTF is a high-Q element with a narrow passband. A typical watch QTF has a $Q \approx 80{,}000$ or higher in vacuum and a $Q \approx 10{,}000$ at normal atmospheric pressure. The resonant frequencies of the mR and the QTF must match for the most efficient sensor operation. Such a frequency-matching design is not straightforward, because the air-filled mR tube and the QTF are acoustically coupled and affect the resonant properties of each other.

To date, two configurations of a QEPAS spectrophone have been reported, both exploiting a longitudinal acoustic resonance in an organ pipe type mR. The first of them shown in Fig. 1a was originally proposed by Kosterev et al. [8, 9] and used in most of the reported QEPAS sensors. The second was recently reported [25] and called by the authors "Off-Beam (OB) QEPAS". In this second configuration the mR is a single tube with a small opening in the middle, and a QTF is coupled to the mR by putting it outside the mR tube near the opening (Fig. 1b). The acoustic coupling is much weaker in this case. This OB-QEPAS configuration will not be considered in this paper.

In the QEPAS review paper [8] published in 2005 the authors assumed that the two parts of the mR (left and right tubes) can be considered in a first approximation as a single tube, neglecting the gap and the QTF between them. Based on such an assumption, each tube was cut to the $l \approx \lambda_s/4$ length, where λ_s is the sound wavelength, to form a half-wave resonator (Fig. 2a). Subsequent research, however, revealed that the detected signal in a mR of such a geometry is much stronger when $l \approx \lambda_s/2$ [26]. This fact suggests

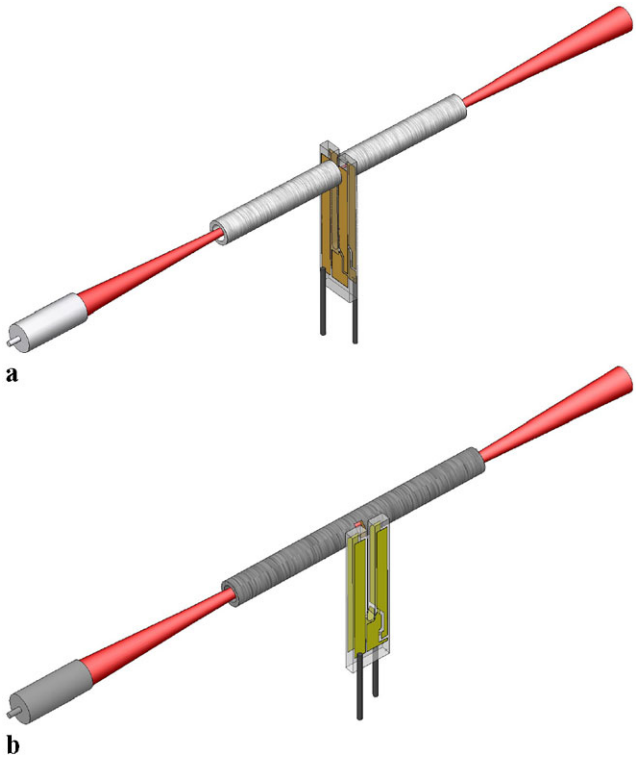

Fig. 1 Two configurations of a QEPAS spectrophone: the most widely used two-tube configuration (**a**) and an OB-QEPAS single-tube configuration (**b**)

that the gap between the tubes is big enough to make them almost independent (Fig. 2b). More detailed studies [27] showed that the optimum length is actually between $\lambda_s/4$ and $\lambda_s/2$ (Fig. 2c) because of the interaction of two resonator tubes and acoustic coupling to the QTF. It was also shown in Ref. [27] that variations in l as small as 0.2 mm have a significant impact on the spectrophone properties. The authors of Ref. [27] varied only the length of the microresonator tubes. In the following section an experimental study of the spectrophone geometry impact on the spectrophone properties and operation is reported, which includes variations of the tube diameter and gaps between the QTF surface and tubes facets. The quartz tuning forks used in this study are identical to those described in [28].

3 Experimental optimization of the microresonator for nitrogen as a carrier gas

The experimental setup for optimization of the mR parameters is shown in Fig. 3. A near-infrared fiber-coupled distributed feedback (DFB) diode laser (JDS Uniphase model CQF935/908-19600) was used as the QEPAS excitation source. The diode laser output was divided in a 1:99 ratio by means of a fiber coupler (ThorLabs 10202A-99-APC). A small fraction of the laser light was sent to a com-

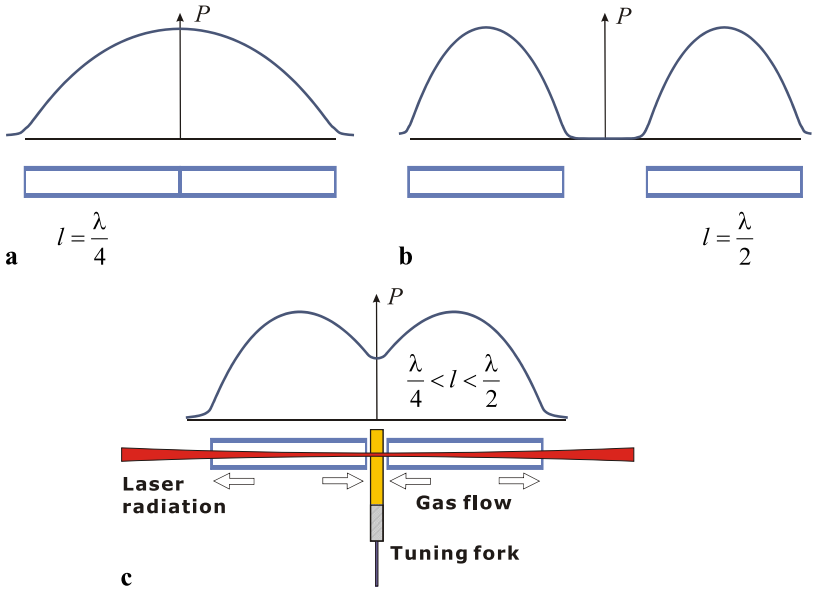

Fig. 2 Acoustic resonance in two tubes: stuck together without gap (**a**); separated by a large gap so that there is no acoustic coupling (**b**); intermediate case—two acoustically coupled tubes with a quartz tuning fork between them (**c**); l is the length corresponding to acoustic resonance in the system, and P is the acoustic pressure

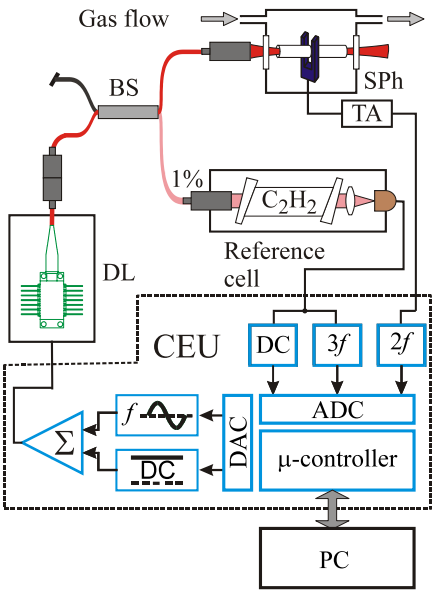

Fig. 3 Schematic diagram of the experimental setup. SPh: spectrophone; BS: 1:99 beam splitter; TA: transimpedance amplifier; DL: diode laser with a temperature controller and current driver; CEU: control electronics unit; f: laser current modulation frequency; DC, $2f$, $3f$: the corresponding components of the electrical signals; ADC: analog-to-digital converter; DAC: digital-to-analog converter; PC: personal computer

mercial fiber-coupled reference module (Wavelength References, Mulino, OR) containing a sealed cell filled with a mixture of 5 Torr C_2H_2 and 145 Torr N_2, a fiber collimator, and a photodiode. The remaining laser power, 46 mW, was directed to a spectrophone consisting of the QTF and two tubes forming the acoustic mR. The spectrophone was placed into a vacuum-tight enclosure (the inner gas volume is $V \sim 1$ cm^3 when the spectrophone is installed) equipped with gas inlet and outlet and two BK7 windows with antireflection (AR) coatings. A calibrated 10 ppmv C_2H_2 in N_2 was used to study the spectrophone photoacoustic sensitivity. The gas flow was set to 100 sccm. A C_2H_2 absorption line at 6529.17 cm^{-1} [29] with 6.31×10^{-7} cm^{-1} peak absorption for 1 ppmv concentration at atmospheric pressure was selected. A control electronics unit (CEU) was employed to measure the resonant frequency f_{QTF}, quality factor Q and resistance R of the QTF, to modulate the laser current at $f_L = 1/2 f_{QTF}$, to lock the laser wavelength to the target absorption line and to measure the current generated by the QTF in response to the photoacoustic signal. A pressure controller (MKS Type 649) was used to maintain the desired pressure in the spectrophone cell.

Both signal and noise should be considered for the correct assessment of the sensor performance. It is theoretically predicted and verified in many experiments that the QEPAS spectrophone noise is primarily determined by the thermal noise of QTF. The QTF noise measured at the transimpedance amplifier output at the resonant frequency f_{QTF} is equal to the thermal noise of the equivalent resistor R [30]

$$\sqrt{\langle V_N^2 \rangle} = R_g \sqrt{\frac{4k_B T \Delta f}{R}}, \tag{1}$$

where $\sqrt{\langle V_N^2 \rangle}$ is the noise rms voltage, Δf is the detection bandwidth (assuming $\Delta f \ll \frac{\pi}{2} \frac{f_{QTF}}{Q}$, the QTF bandwidth), and T is the QTF temperature. The gain resistor $R_g = 10$ MΩ also introduces noise with a spectral density $\sqrt{4k_B T R_g}$, added to the QTF noise in quadrature. However, it is $\sqrt{R_g/R}$ times lower than the QTF noise and can be usually neglected for typical values of $R \sim 10$ to 200 kΩ. R represents QTF oscillator losses and is related to other

QTF parameters as $R = \frac{1}{Q}\sqrt{\frac{L}{C}}$, where L is an equivalent inductance representing the QTF oscillator equivalent mass, and C represents the inverse force constant. Both L and C do not change more than 0.1% due to interaction with gas. Therefore, when a QTF is integrated into different spectrophones, the signal-to-noise ratio (SNR) can be estimated as the ratio of the signal to $\sqrt{Q}$.

Figure 4 displays the SNR comparison for several mR configurations. The scaling factor K for a fixed T is constant for a given QTF. The gaps between a QTF and mR tubes are consistently 50 µm. The distance from the QTF tips to the mR tubes' axis is 0.7–0.9 mm. Such a variation in this parameter does not noticeably impact the signal [28, 31]. The best SNR is achieved with $l = 4.4$ mm tubes. This length is significantly shorter than the half-wavelength of sound, $\lambda_s/2 = 5.2$ mm, calculated based on the speed of sound of 340 m/s in pure nitrogen at 20°C. Such a deviation qualitatively agrees with an assumed pressure distribution in Fig. 2. With tubes of $l = 5.1$ mm which are detuned furthest from resonance the SNR increases upon reducing the tube diameter. The resonant effects in the mR of this configuration are not strongly pronounced. Therefore, the volume of the excited gas becomes the primary factor and causes the signal to increase when the absorbed optical energy is distributed over a smaller amount of gas. For the optimum tube length of $l = 4.4$ mm the effects of acoustic resonance dominate. The Q factor of the gas-filled organ pipe resonator increases with its diameter, resulting in a higher acoustic pressure and SNR.

Figure 5 presents the changes in the measured QTF parameters when it is coupled to the mR. The decrease of Q provides a measure of acoustic coupling between the QTF and the mR, because the high-Q QTF is losing energy primarily via coupling to the low-Q mR oscillator. Changes of the resonant frequency are less reliable because of some initial scatter among QTFs. However, a general trend exists that a QTF integrated into a mR has a higher natural frequency. This observation indicates that an additional force constant is added due to acoustic coupling. This plot also indicates that thicker mR tubes provide stronger acoustic coupling (lower Q). The tubes with larger inner diameter match the QTF frequency when cut to a shorter length. This result qualitatively agrees with Fig. 2, because with a larger tube diameter the gap between two mR tubes becomes less important and the system moves closer to the case depicted in Fig. 2a. The largest drop in Q-factor is observed for $l = 3.9$ mm and ID = 0.84 mm, the largest tested inner diameter. This configuration has advantages of easier optical alignment of the excitation radiation through wider and shorter tubes, and faster sensor response time $\tau = Q/\pi f_0$. An advantage of the fast response with a matched mR was used in [32]. On the other hand, spectrophones with strongly acoustically coupled mR and QTF are more sensitive to

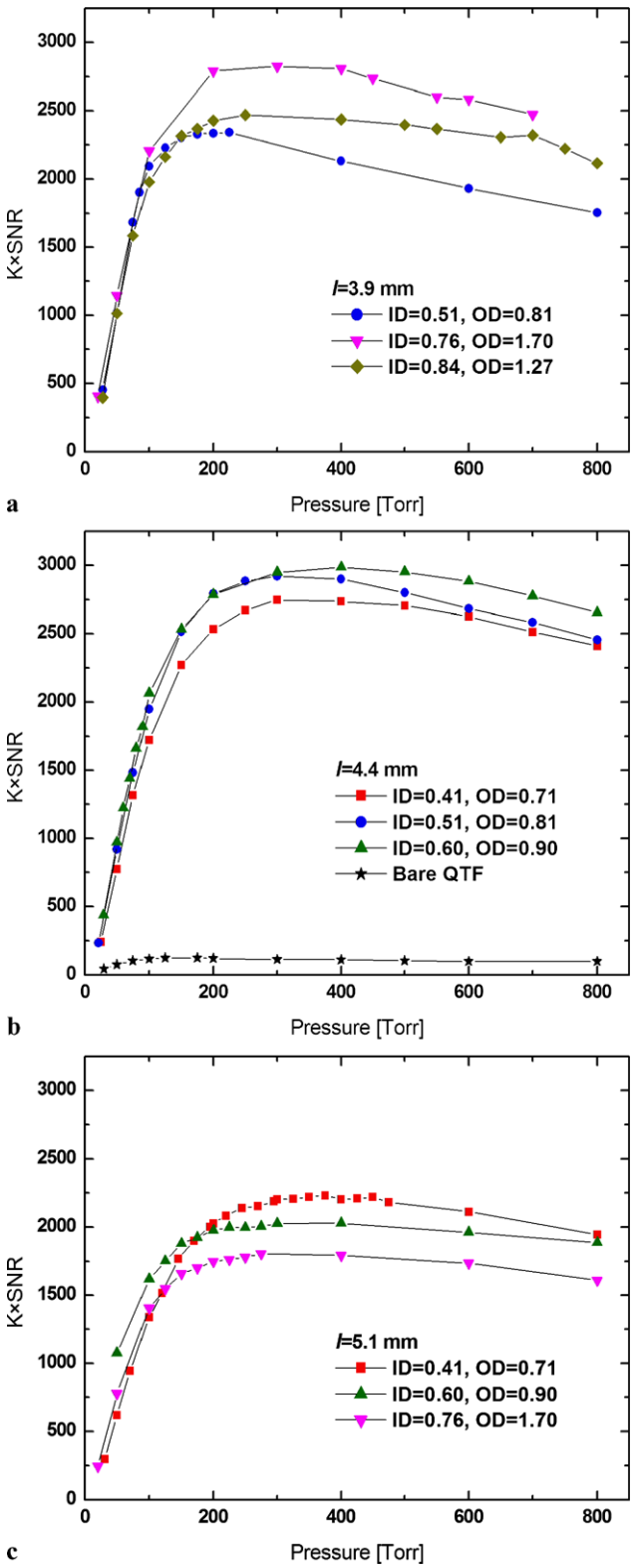

Fig. 4 Signal-to-noise ratio as a function of the pressures in different QEPAS spectrophone configurations. l: length of each spectrophone tube; ID, OD: inner and outer diameter of the tube in mm. (**a**) 3.9 mm long tubes, (**b**) 4.4 mm long tubes and bare QTF, (**c**) 5.1 mm long tubes

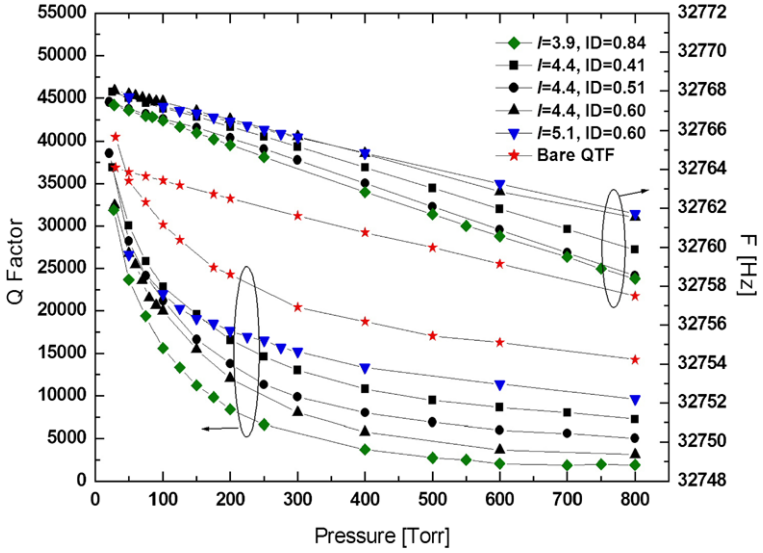

Fig. 5 Q-factor and frequency of the QTF as a function of the pressure for different tube lengths and diameters. ID, l: inner diameter and length of the tubes in mm

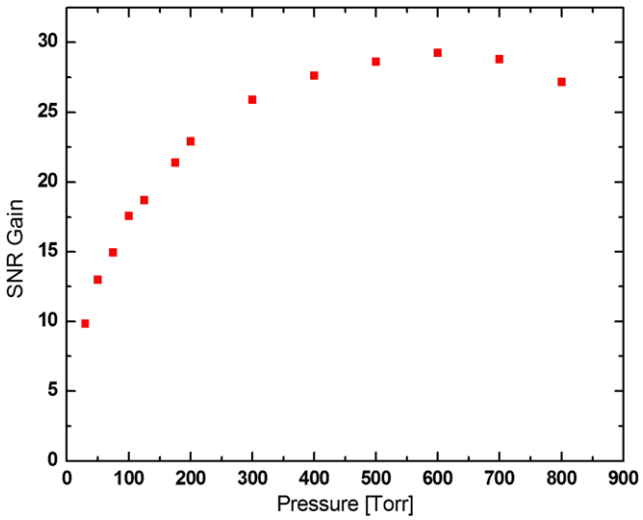

Fig. 6 Gain in the SNR due to the microresonator with respect to the bare QTF. The microresonator dimensions are: $l = 4.4$ mm, ID = 0.6 mm, OD = 0.9 mm, gap between the tubes facets and the QTF surface 50 μm

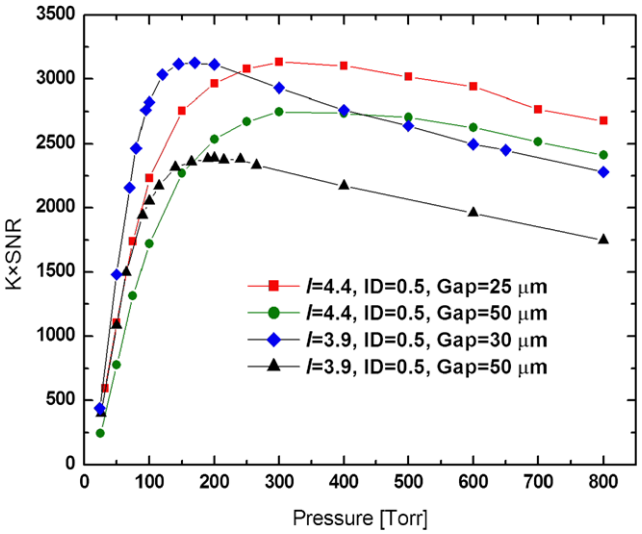

Fig. 7 Signal-to-noise ratio as a function of gas pressure for 25 μm, 30 μm and 50 μm gaps between the tube facets and the QTF surface. ID, l: inner diameter and length of the tubes in mm

environmental acoustic noise. Instead of a QTF, which is acoustically a quadrupole, the acoustic background is received by the mR which is an acoustic dipole, and the acceptance bandwidth is higher because of the reduced Q-factor.

In Fig. 4b, in addition to the mR data, we present the SNR measured with only a QTF (no mR), and Fig. 6 shows the improvement in SNR achieved due to the mR when the gaps between the QTF and the tubes are 50 μm each, $l = 4.4$ mm, and ID = 0.60 mm. This gain is ∼30 in the 500–700 Torr pressure range. A normalized noise-equivalent absorption coefficient at atmospheric pressure for the used C_2H_2 line was found to be 3.3×10^{-9} cm^{-1} W/Hz$^{1/2}$ for these mR geometrical parameters. The same sensitivity was reported in [27] for the 6528.8 cm^{-1} NH_3 absorption peak.

The gaps size between the QTF and the mR tubes is a parameter which is difficult to control during the spectrophone assembly, but it has a significant effect on the spectrophone performance. With a large gap, the diverging flow from the mR cannot efficiently push against the QTF prong. Figure 7 shows the SNR comparison for different gaps. With a 4.4 mm-long 0.5 mm-inner-diameter tube, the SNR is improved 13% for pressure 200–800 Torr when the gap is reduced from 50 to 25 μm. With the 3.9 mm-long 0.5 mm-inner-diameter tube, the SNR is improved 27% for pressures from 100 Torr to 800 Torr when the gap is reduced from 50 to 30 μm.

4 Effects of the changing carrier gas

Interaction between the QTF and the mR is dependant upon the mismatch between their natural resonant frequencies. The resonant frequency of the QTF is primarily determined by the mechanical properties of the quartz crystal and does not significantly change in the presence of a gas. To the contrary, the mR resonant frequency is directly proportional to the speed of sound in the gas and therefore is affected by the bulk gas composition. To observe this effect, we mixed gases from two cylinders, the first containing 5% CO_2 in N_2, and the second with pure CH_4. The QEPAS signal from CO_2 was monitored. For that purpose, a near-infrared DFB diode laser (FITEL model FOL 15 DCWD-A82-19070) and CO_2 reference gas module (Wavelength References, Mulino, OR) were used instead of the laser and the reference gas module for C_2H_2 in Fig. 3. A CO_2 absorption line at 6361.25 cm^{-1} [29] with 1.39×10^{-5} cm^{-1} peak absorption for 1% concentration at atmospheric pressure was employed to excite CO_2. The speed of sound in pure CH_4 is ~430 m/s at 20°C. Therefore, its addition to N_2 increases the speed of sound in the gas and shifts the mR resonance to a higher frequency.

The measurements were carried out at atmospheric pressure with two different microresonators. The first resonator with $l = 4.4$ mm and ID = 0.5 mm was believed to be of the optimum length in the nitrogen carrier gas, its frequency matching the 32,760 Hz resonant frequency of the QTF. The second mR with $l = 5.1$ mm and ID = 0.76 mm was presumably detuned from 32,760 Hz to a lower frequency in N_2 carrier (Fig. 8). Figure 9a shows the measured Q-factor of the QTF. When the CH_4 concentration increases, the resonant frequency of the $l = 4.4$ mm mR is detuned from the QTF, as shown in Fig. 8. As a result, the transfer of vibrational energy from the QTF to a high-loss mR becomes less efficient, and the measured Q-factor of the QTF increases. The situation is just the opposite for the $l = 5.1$ mm mR, in which case the resonances of mR and QTF get closer with increasing CH_4 concentration. Figure 9b shows the QEPAS signal normalized to the QTF Q-factor and CO_2 concentration. The resulting number reflects the force acting on the QTF (at a fixed CO_2 concentration), which is in turn proportional to the acoustic pressure. The rising part (0 to 5% CH_4) is due to the vibrational–translational (V–T) relaxation kinetics. The V–T relaxation of CO_2 in dry N_2 is known to be slow. The translational gas temperature cannot follow fast changes in the laser induced molecular excitation rate. Thus the generated photoacoustic wave is weaker than it would be in case of instantaneous V–T relaxation. The addition of CH_4 to a nitrogen carrier gas increases the energy transfer rate from the initially excited ro-vibrational state of CO_2 into translational motion of gas molecules, increasing the magnitude of acoustic signal, until the $\omega\tau < 1$ condition is met (where $\omega = 2\pi f_{QTF}$ and τ is a characteristic V–T relaxation time). With more CH_4 added, the ef-

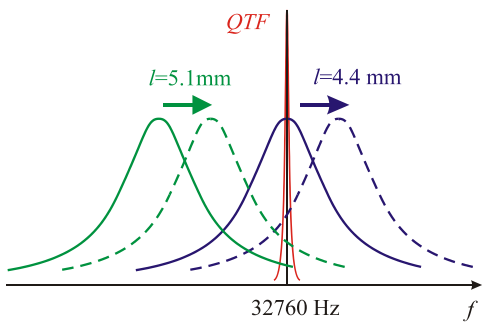

Fig. 8 A qualitative representation of the mR and QTF resonances. Solid curves show the mR resonances in nitrogen. Initially, the $l = 4.4$ mm mR has a resonant frequency coinciding with the QTF frequency. The *arrows* show the direction of the resonant frequency shift when CH_4 is added, increasing the speed of sound

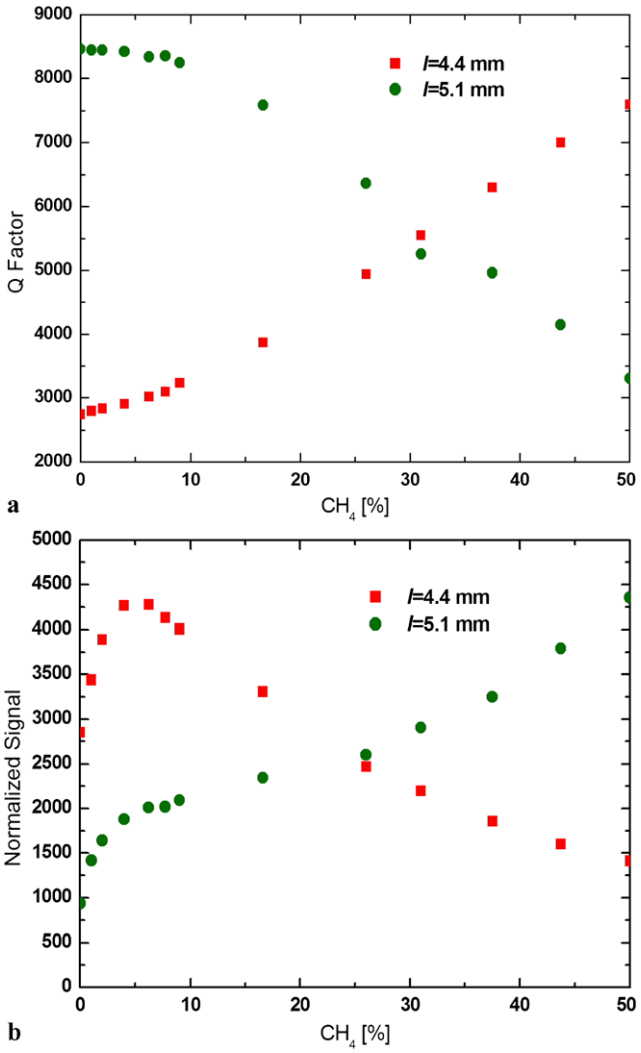

Fig. 9 (**a**) Q-factor of the QTF as a function of CH_4 concentration for the 4.4 mm-long tubes and the 5.1 mm-long mR tubes. (**b**) QEPAS signal detected from CO_2 normalized to the CO_2 concentration and the QTF Q-factor as a function of CH_4 concentration for the same tubes

ficiency of the acoustic excitation of the $l = 4.4$ mm mR decreases as the optical excitation frequency (kept equal to the resonant frequency of the QTF) is detuned from the mR natural frequency. The opposite situation is observed for the $l = 5.1$ mm mR. These experiments demonstrate that changing the gas composition is an efficient technique of validating the frequency match between mR and QTF in the QEPAS spectrophone.

5 Side-by-side comparison of QEPAS and conventional PAS spectrophones

A comparison of QEPAS and conventional PAS based on published data is difficult because of variations in experimental conditions, incomplete reports, and different criteria used to assess the sensor performance. Therefore, we performed a side-by-side comparison of the QEPAS spectrophone and a state-of-the-art conventional PAS (CPAS) differential detector.

For this comparison we used a QEPAS spectrophone assembled by Achray Photonics, Inc. in a telecom-style package, with the near-IR laser radiation delivered via a single mode optical fiber and subsequently focused by means of a GRIN lens (Fig. 10). The mR consisted of two $l = 4.4$ mm, ID = 0.51 mm hypodermic tubes, positioned 0.6 mm below the QTF tips. The CPAS sensor design and its performance as evaluated with a pulsed CO_2 laser were reported in [33]. Dimensions and other relevant parameters of the QEPAS and CPAS spectrophones are summarized in Table 1. We used two gases to evaluate the PAS sensors: (1) 10 ppmv C_2H_2 in N_2 (6529.17 cm^{-1} absorption line), and (2) pure CO_2 (6493.42 cm^{-1} absorption line). Based on our previous experience, C_2H_2 has a fast V–T relaxation rate, which can be considered instantaneous on the $1/f_0$ time scale. The V–T relaxation of the initially excited $3\nu_3 + \nu_1$ state of CO_2 is slow or incomplete, as indicated by the measured QEPAS sensitivity.

The measurements were performed at atmospheric pressure with 100 sccm gas flow, using $2f$ wavelength modulation technique. The results are summarized in Table 2. For C_2H_2, the QEPAS detection sensitivity is 1.3 times higher than the CPAS sensitivity; for CO_2, the QEPAS sensitiv-

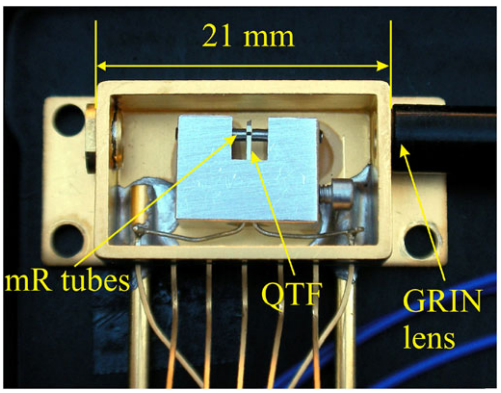

Fig. 10 Fiber-coupled QEPAS spectrophone for near-IR spectral range

Table 1 Parameters of the QEPAS and CPAS spectrophones

	QEPAS	CPAS
Spectrophone dimensions	21 × 12.7 × 8.5 mm	$l = 136$ mm, ø56.5 mm
Resonator volume	2 mm^3	4500 mm^3
Optical path length	9 mm	90 mm
Resonant frequency	32,735 Hz in N_2	1787 Hz in N_2
	32,733 Hz in CO_2	1367 Hz in CO_2
Q-factor	3630 in N_2	49 in N_2
	7930 in CO_2	56 in CO_2
Maximum flow rate	400 sccm	1200 sccm

Table 2 Sensitivity comparison between QEPAS and CPAS

	10 ppm C_2H_2 in N_2		Pure CO_2	
	QEPAS	CPAS	QEPAS	CPAS
Signal, μV	6280	46	13880	413
Noise, μV	53	0.49	74	0.91
SNR	119	94	188	455
Laser power, mW	37.2	39.0	21.1	24.3
NNEAC, $cm^{-1}W/Hz^{1/2}$	4.1×10^{-9}	5.4×10^{-9}	16.0×10^{-9}	7.6×10^{-9}

NNEAC: normalized noise-equivalent absorption coefficient
Equivalent noise detection bandwidth is 0.833 Hz

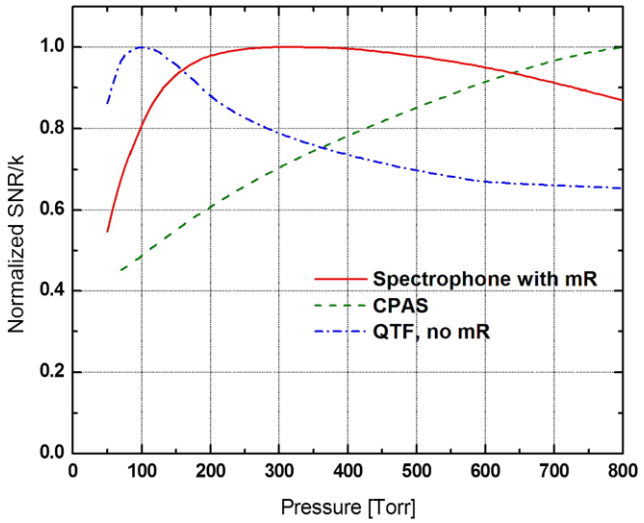

Fig. 11 Curves summarizing the results on sensitivity as a function of pressure acquired in this study for different spectrophones. The measurements were performed for 10 ppm C_2H_2 in N_2. *Vertical axis* is the measured SNR divided to the peak absorption of C_2H_2 that was calculated based on HITRAN data. Each *curve* is normalized to its maximum value

ity is 2.1 times lower than the CPAS sensitivity. The reason for a sharper sensitivity drop of QEPAS sensitivity for a slower relaxing CO_2 is a 24 times higher modulation frequency compared to CPAS.

We also studied the SNR for 10 ppm C_2H_2 as a function of the total gas pressure using three spectrophones: (1) configuration of Fig. 1a, (2) CPAS cell, and (3) QTF without mR. Smoothed values of the SNR divided to the peak absorption coefficient of C_2H_2 at 6529.17 cm^{-1} at each pressure are shown in Fig. 11. Each curve is normalized to its maximum value. The Q-factor of the gas-filled CPAS resonator increases with the total gas pressure, while the Q-factor of a QTF without mR decreases, resulting in the observed behavior of the SNR. A QEPAS spectrophone with a mR combines the properties of these two elements, the increasing Q of the mR partially compensating the decreasing Q of the QTF. The drop of the QTF sensitivity below 100 Torr is probably associated with the V–T relaxation dynamics.

6 Conclusions

It follows from our study that the sensitivity (signal-to-noise ratio) of QEPAS can be increased 1.5–2 times at atmospheric pressure when the mR tubes are cut to the correct length to match the QTF resonant frequency in a particular carrier gas. Another advantage of the QEPAS spectrophone with matched resonances of the QTF and mR is the up to 8–10 times shorter response time, corresponding to the reduced Q-factor of the spectrophone. The reduced Q-factor is also responsible for the lower spectrophone noise level, which is the main factor in improving the SNR. Thus, the practical realization of the matched-resonances spectrophone sensitivity advantages requires careful EMI shielding and electronics design. The matched-resonances spectrophone parameters (resonant frequency, quality factor, and responsivity) are sensitive to the speed of sound, which in turn can be affected by the gas temperature and bulk composition. Therefore, in a changing environment the use of spectrophones with intentionally detuned mR and QTF frequencies may be advantageous, regardless of the reduced sensitivity. Besides, the matched-resonances spectrophone is expected to be more sensitive to environmental acoustic noise because the mR acts as an acoustic antenna, although we did not observe excess noise in laboratory experiments.

Acknowledgements The Rice University group acknowledges financial support from a National Science Foundation ERC MIRTHE award, a grant C-0586 from The Welch Foundation and a grant from the National Aeronautics and Space Administration.

References

1. R.F. Curl, F. Capasso, C. Gmachl, A.A. Kosterev, B. McManus, R. Lewicki, M. Pusharsky, G. Wysocki, F.K. Tittel, Chem. Phys. Lett. **487**, 1 (2010)
2. M. Troccoli, L. Diehl, D.P. Bour, S.W. Corzine, N. Yu, C.Y. Wang, M.A. Belkin, G. Hofler, R. Lewicki, G. Wysocki, F.K. Tittel, F. Capasso, J. Lightwave Technol. **26**, 3534 (2008)
3. A.A. Kosterev, G. Wysocki, Y.A. Bakhirkin, S. So, R. Lewicki, F.K. Tittel, R.F. Curl, Appl. Phys. B **90**, 165 (2008)
4. A.A. Kosterev, F.K. Tittel, G. Bearman, in *Proceedings of the 2008 Int. Conference on Environmental Systems*, Published by SAE as MS 08ICES-0031 (2008)
5. J.S. Pilgrim, J. Kutzner, W.R. Wood, in *Proceedings of the 2007 Int. Conference on Environmental Systems*, Published by SAE as MS 2007-01-3152 (2007)
6. M.R. McCurdy, Y.A. Bakhirkin, G. Wysocki, R. Lewicki, F.K. Tittel, J. Breath Res. **1**, 014001 (2007)
7. G. Wysocki, Y.A. Bakhirkin, S. So, F.K. Tittel, C.J. Hill, R.Q. Yang, M.P. Fraser, Appl. Opt. **46**, 8202 (2007)
8. A.A. Kosterev, F.K. Tittel, D. Serebryakov, A.L. Malinovsky, I. Morozov, Rev. Sci. Instrum. **76**, 1 (2005)
9. A.A. Kosterev, Y.A. Bakhirkin, R.F. Curl, F.K. Tittel, Opt. Lett. **27**, 1902 (2002) ()
10. J.-M. Friedt, E. Carry, Am. J. Phys. **75**, 415 (2007)
11. K. Liu, J. Li, L. Wang, T. Tang, W. Zhang, X. Gao, W. Chen, F.K. Tittel, Appl. Phys. B **94**, 527 (2009)
12. A.A. Kosterev, Y.A. Bakhirkin, F.K. Tittel, S. McWhorter, B. Ashcraft, Appl. Phys. B **92**, 103 (2008)
13. C.W. Van Neste, L.R. Senesac, T. Thundat, Appl. Phys. Lett. **92**, 234102 (2008)
14. R. Lewicki, G. Wysocki, A.A. Kosterev, F.K. Tittel, Appl. Phys. B **87**, 157 (2007)
15. R. Lewicki, G. Wysocki, A.A. Kosterev, F.K. Tittel, Opt. Express **15**, 7357 (2007)
16. A.K. Ngai, S.T. Persijni, D. Lindsay, A.A. Kosterev, P. Groß, C.J. Lee, C.M. Cristescu, F.K. Tittel, K.J. Boller, F.J. Harren, Appl. Phys. B **89**, 123 (2007)
17. Y.A. Bakhirkin, A.A. Kosterev, R.F. Curl, F.K. Tittel, D.A. Yarekha, L. Hvozdara, M. Giovannini, J. Faist, Appl. Phys. B **82**, 149 (2006)

18. A.A. Kosterev, T.S. Moseley, F.K. Tittel, Appl. Phys. B **85**, 295 (2006)
19. G. Wysocki, A.A. Kosterev, F.K. Tittel, Appl. Phys. B **85**, 301 (2006)
20. A.A. Kosterev, Y.A. Bakhirkin, F.K. Tittel, Appl. Phys. B **80**, 133 (2005)
21. A.A. Kosterev, F.K. Tittel, Appl. Opt. **43**, 6213 (2004)
22. D. Weidmann, A.A. Kosterev, F.K. Tittel, N. Ryan, D. McDonald, Opt. Lett. **29**, 1837 (2004)
23. A. Miklós, P. Hess, Z. Bozóki, Rev. Sci. Instrum. **72**, 1937 (2001)
24. T. Schmid, Anal. Bioanal. Chem. **384**, 1071 (2006)
25. K. Liu, X.Y. Guo, H.M. Yi, W.D. Chen, W.J. Zhang, X.M. Gao, Opt. Lett. **34**, 1594 (2009)
26. S. Schilt, A.A. Kosterev, F.K. Tittel, Appl. Phys. B **95**, 813 (2009)
27. D.V. Serebryakov, I.V. Morozov, A.A. Kosterev, V.S. Letokhov, Quantum Electron. **40**, 167 (2010)
28. N. Petra, J. Zweck, A.A. Kosterev, S. Minkoff, D. Thomazy, Appl. Phys. B **94**, 673 (2009)
29. L.S. Rothman, A. Barbe, D.C. Benner, L.R. Brown, C. Camy-Peyret, M.R. Carleer, K. Chance, C. Clerbaux, V. Dana, V.M. Devi, A. Fayt, J.M. Flaud, R.R. Gamache, A. Goldman, D. Jacquemart, K.W. Jucks, W.J. Lafferty, J.Y. Mandin, S.T. Massie, V. Nemtchinov, D.A. Newnham, A. Perrin, C.P. Rinsland, J. Schroeder, K.M. Smith, M.A.H. Smith, K. Tang, R.A. Toth, J. Vander Auwera, P. Varanasi, K. Yoshino, J. Quant. Spectrosc. Radiat. Transf. **82**, 5 (2003)
30. R.D. Grober, J. Acimovic, J. Schuck, D. Hessman, P.J. Kindlemann, J. Hespanha, A.S. Morse, K. Karrai, I. Tiemann, S. Manus, Rev. Sci. Instrum. **71**, 2776 (2000)
31. S.L. Firebaugh, F. Roignant, E.A. Terray, in *Proceedings Comsol Conf.*, Boston, October 8–10, 2009
32. A.A. Kosterev, P. Buerke, L. Dong, M. Reed, T. Day, F.K. Tittel, Appl. Phys. B (2010). doi:10.1007/s00340-010-3975-0
33. C.-M. Lee, K.V. Bychkov, V.A. Kapitanov, A.I. Karapuzikov, Y.N. Ponomarev, I.V. Sherstov, V.A. Vasiliev, Opt. Eng. **46**, 064302 (2007)